J. Fluid Mech. (2003), *vol.* 477, *pp.* 175–200.
DOI: 10.1017/S0022112002003117 Printed in the United Kingdom

The stability of ink-jet printed lines of liquid with zero receding contact angle on a homogeneous substrate

By P. C. DUINEVELD

Philips Research, Prof. Holstlaan 4, 5656 AA Eindhoven, The Netherlands

(Received 15 March 2002 and in revised form 5 September 2002)

We have studied the stability of ink-jet printed lines of liquid with zero receding contact angle on a homogeneous substrate. Such lines can become unstable by forming a series of liquid bulges, at various wavelengths, connected by a ridge of liquid. The instability was studied with a simple dynamic model. It was shown that the line becomes unstable when the contact angle of the liquid with the substrate is larger than the advancing contact angle. This condition, however, is not a sufficient condition. When the transported flow rate is sufficiently small compared to the applied flow rate a printed line can be shown to be stable, i.e. the width of the printed line is constant. This was found to depend on the advancing contact angle of the liquid over the substrate.

1. Introduction

In the electronics industry there are numerous products where patterns of a functional material have to be applied. At present the standard technology used to make these patterns is photo-lithography, which consists of several steps. First, a continuous layer of the functional material is applied. Then a uniform photo-resist layer is spin-coated on top of the functional material, where the resist is cross-linked during spinning. With a photo-mask a light pattern is applied on the resist, which breaks up the cross-linked bonds that are in contact with the light. After rinsing, a resist pattern remains. Now the substrate is ready for an etching step, where the resist pattern protects the functional material from the etching solution. Finally the resist is stripped and a pattern of the functional material remains. In spite of the many steps involved, photo-lithography is a very robust process and it is succesfully used to make patterns as small as 0.1 μm for the IC industry. On the other hand patterns of order 100 μm are also made with this technology.

At present the electronics industry is interested in using selective patterning techniques to replace photo-lithography in flat display applications, where the substrate is non-porous.

With microcontact printing a stamp is used to print patterns of a monolayer on a substrate. The stamp is made with photo-lithographic techniques and the printed patterns can be as small as sub-micron, as is described in the review by Xia & Whitesides (1998). The monolayer can be used as a sacrificial mask or to locally vary the wetting properties. With this printing technique the number of steps in making a pattern can be substantially reduced. Although microcontact printing is a very interesting technique it is still in the research phase.

Ink-jet printing is, due to the ongoing miniaturization and flexibility, a very promising additive patterning technique with a current minimum pattern size of order 30 μm. Although this is considerably larger than photo-lithography there are, due to its additive character, very interesting applications such as printing of metal tracks, colour filters for LCD displays and also printing of polymer solutions for light-emitting polymer displays such as described in Shimoda *et al.* (1999) and Duineveld *et al.* (2001) and polymer electronics, such as reported by Sirringhaus *et al.* (2000).

Nowadays ink-jet printing is very common in the graphics industry, but it has not yet entered mass manufacturing in the electronics industry as the demand on the quality of the printed patterns is much tighter. It is expected, however, that within a few years time the technology will also be used in the electronics industry.

The subject of this paper is ink-jet printing of a line of liquid on a flat homogeneous substrate. It is well known that a line of liquid on a flat substrate can be unstable, depending on the boundary conditions of the moving contact line. The first theoretical work was performed by Davis (1980) and Sekimoto, Oguma & Kawasaki (1987). An experimental verification including a nice one-dimensional model was presented by Schiaffino & Sonin (1997). When the contact angle θ of the liquid with the substrate is constant and the contact line is free to move, a liquid line is unstable for all θ. An example of such a boundary condition is the printing of a line of water on a flat substrate reported by Schiaffino & Sonin (1997). With a fixed width the line will be unstable when $\theta > \pi/2$. This boundary condition was demonstrated by Schiaffino & Sonin (1997) when printing hot melted drops of wax on a cold substrate. Both boundary conditions are extensions of the classical instability of a cylinder of liquid studied by Rayleigh (1878).

In this paper the boundary condition of the liquid with the substrate is different from those previously reported. Our liquid has a zero receding contact angle with the substrate, i.e. the liquid does not dewet the substrate. The advancing contact angle of the liquid is finite, hence the liquid is said to partly wet the substrate. This contact angle hysteresis gives rise to another type of instability. In general, suspensions of small spheres in a solvent can have a zero receding contact angle. Examples of this are given by Deegan (2000).

We present several experiments with a model liquid on substrates with different surface conditions. Depending on the substrate and experimental conditions three different patterns were observed, figure 1. Figure 1(*a*) is obtained with a boundary condition of a (nearly) constant contact angle of the liquid with the substrate. The printed line breaks up, as expected, into separate drops. This instability can be described with the known theory, see Davis (1980) and Schiaffino & Sonin (1997). The other experiments were performed with a zero receding contact angle and two different advancing contact angles. Now a line may become unstable by forming a series of liquid bulges connected by a ridge of liquid, figure 1(*b*). The printed liquid lines are not always unstable however and we also show experimentally stable lines, figure 1(*c*).

We have studied the growth rate of a bulge with a simple dynamic model and found a stability criterion for an ink-jet printed liquid line which shows reasonably good agreement with theory. With this simple model the distance between the bulges can also be calculated and was found to be in reasonable agreement with experimental results.

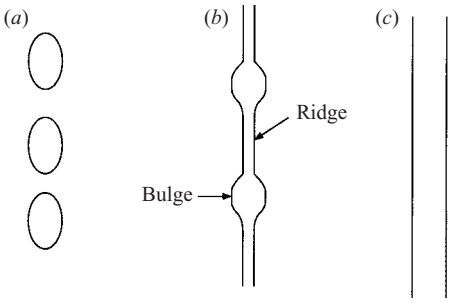

FIGURE 1. Different modes of a printed line on a substrate; (*a*) the line breaks up into individual droplets; (*b*) the line breaks up into liquid bulges connected by a ridge of liquid; (*c*) stable printed line.

2. Experimental set-up

The model liquid is a small amount of the conducting polymer, poly(3,4-ethylenedioxythiophene) doped with polystyrene sulphonic acid (PEDOT/PSS, Baytron P from Bayer, Krefeld, Germany) dissolved in water. This polymer is used in the fabrication of light-emitting polymer displays and plastic electronics, e.g. Sirringhaus *et al.* (2000) and Duineveld *et al.* (2001). It can be described very well as a suspension of polymer spheres in the solvent. In this paper we refer to this material by its common name: Pedot. The surface tension, σ, of Pedot was measured to be close to that of water: $0.07\,\mathrm{N\,m^{-1}}$. The dynamic viscosity, μ, of the liquid used in the experiments was 20 cP at room temperature.

Drops were generated with a MicroDrop single-nozzle piezo-electric drop-on-demand ink-jet system with a specified nozzle diameter of 50 μm. The diameter of an ejected Pedot drop, D, as it leaves the nozzle, was found to be $D = 67.4 \pm 1.0\,\mu\mathrm{m}$, giving a drop volume, V_d of 160 pl. The velocity of the drops as they leave the nozzle $\approx 2\ \mathrm{m\ s^{-1}}$. The ink-jet head was positioned $\approx 1\,\mathrm{mm}$ from the substrate and kept fixed during experiments. The substrate was moving on a computer controlled x-y translation stage, with a variable speed of between 1 and $30\,\mathrm{mm\,s^{-1}}$. An encoder signal from the x-y stage gave a trigger to the droplet-on-demand ink-jet system. In this way drops could be placed on the substrate with a variable inter-drop distance: Δx. This is the centre-to-centre distance on the substrate between successively landing drops, i.e. it is the tail-to-tail distance between the drops on the substrate. With our system both the substrate velocity U and Δx can be independently varied. This is done by changing the droplet frequency. Note that the x-y stage is the master and the droplet-on-demand ink-jet system the slave.

In the experiments the drops were printed on 6 in. square glass substrates. In order to vary the wettability of the liquid on substrate we have spin-coated on top of the glass plate a standard photo-resist layer, a few microns thick which was given different surface treatments: used as received, put in a UV–ozone oven, or treated by a CF_4 plasma. Both the advancing and receding contact angles of the liquid with the different substrates were measured. The advancing contact angle, θ_a, is defined as the contact angle of an advancing liquid front with the substrate, while the receding contact angle, θ_r, is the contact angle of a receding liquid front. These contact angles were determined by the quasi-static technique of slowly forming a mm sized drop of liquid through a needle onto the substrate, table 1. For the reader interested in this field we refer to the reviews by Dussan V. (1979) and Blake (1993). The UV–ozone

Type	Substrate	θ_a	θ_r
I	UV–ozone treated (5 minutes) resist	0.42 ± 0.04	0
II	'Standard', non-treated resist	1.15 ± 0.04	0
III	CF_4 treated resist	1.7 ± 0.04	0.56 ± 0.04

TABLE 1. Contact angles (in rad) of Pedot on the different substrate types.

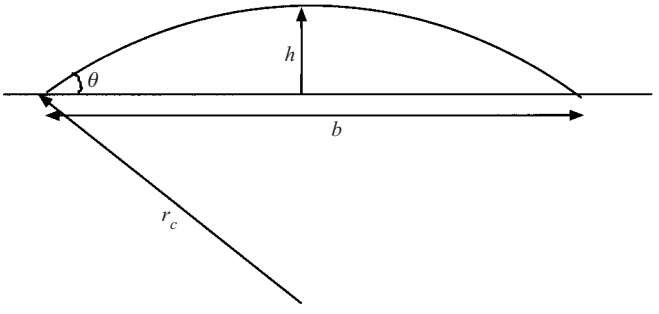

FIGURE 2. Contact angle of a liquid with a solid.

treatment is a standard way to lower the advancing contact angle of the liquid. By increasing the time of the treatment it was found that θ_a was decreased to very low values. With the CF_4 treatment a monolayer of a fluorinated moiety is put on the surface, which increases the advancing contact angle of the liquid with the substrate. The Pedot did not dewet the UV–ozone treated and standard resist plates, while on the CF_4 treated resist it has a finite receding contact angle. The surface treatment of the spin-coated resist plates has the advantage that the roughness of the surface is negligible and is identical for every plate. Note that the substrates used in the experiments are non-porous, which is different from the graphics industry, but similar to substrates used in the electronics industry.

When the drops are printed at a large inter-drop distance, Δx, they will land on the substrate as individual drops. As Δx decreases the individually printed drops will merge to a line. The length of an ink-jet printed line was 30 mm in our experiments and the printed drops were observed with a standard CCD camera.

To describe the experimental results we discuss here the shape of stable lines and drops on a substrate. Due to the small dimensions in the problem it can be shown that the influence of gravity is negligible compared to the surface tension, σ. The standard non-dimensional number to describe this effect is the Bond number, defined here as $Bo = \rho g D^2/\sigma$, where ρ is the density, g the acceleration due to gravity and the diameter of the droplet, D, is the typical length scale in the problem. This gives $Bo < 10^{-3}$; hence the cross-section of a printed drop or line can be described as a truncated circle, where the angle θ is the contact angle of the liquid with the substrate, figure 2. When the liquid is in equilibrium with the solid substrate the contact angle, θ, is given by

$$\cos\theta = \frac{\gamma_{sv} - \gamma_{sl}}{\sigma}, \tag{1}$$

where γ_{sv} and γ_{sl} are the substrate–vapour and substrate–liquid energies per area.

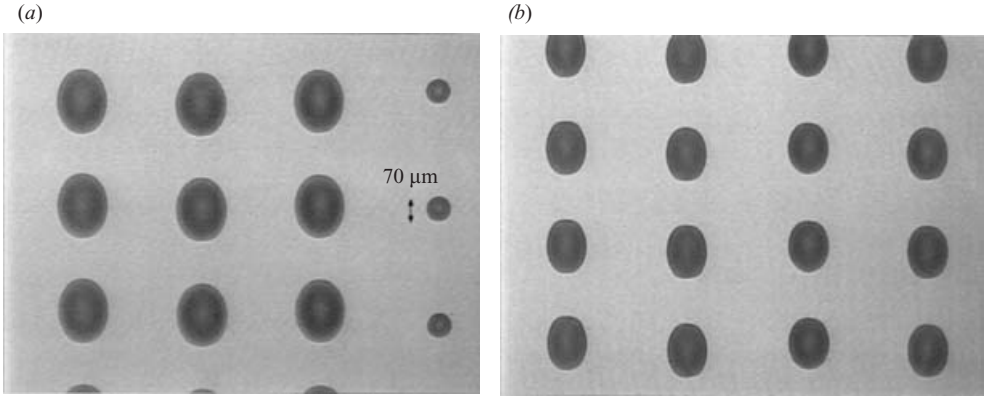

FIGURE 3. Results of ink-jet printed unstable lines on CF_4-treated resist substrates with different inter-drop distances and a substrate velocity of $5\,\mathrm{mm\,s^{-1}}$: (*a*) 30 μm inter drop distance (note the individually printed liquid drops with a diameter of 70 μm); (*b*) 50 μm inter-drop distance.

To describe a line a dimensionless width $b^* = b/\sqrt{S}$ is defined, where S is the area of the cross-section. We have

$$b^* = \frac{2\sin\theta}{\sqrt{\theta - \sin\theta\cos\theta}}. \tag{2}$$

With the standard relations for a truncated circle the functional behaviour for the height h and the radius of curvature r_c as a function of θ can be found.

The area of the liquid cross-section, S, of a stable printed liquid line is given by

$$S = \frac{V_d}{\Delta x}, \tag{3}$$

where V_d is the volume of an individually printed drop, here 160 pl.

For a single printed drop the shape can be derived in a similar way. Here we define the dimensionless width of the drop $b_0^* = b_0/D$, where b_0 is the width of a cross-section of the drop on the substrate. The relation for b_0^* is

$$b_0^* = \left(\frac{4\sin^3\theta}{(1-\cos\theta)^2(2+\cos\theta)}\right)^{1/3}. \tag{4}$$

When the width of a printed drop on the substrate is measured and the volume of the drop is known, the contact angle of the liquid with the substrate can be calculated.

3. Experimental results of ink-jet printed lines on a substrate with finite receding contact angle

Here, the experiments performed on type III substrates, i.e. treated with CF_4 are described. Typical examples are shown in figure 3. In all figures showing experimental results in this paper a top view of the dried polymer pattern is shown. Both figures 3(*a*) and 3(*b*) were printed with a substrate speed of $5\,\mathrm{mm\,s^{-1}}$. In figure 3(*a*) we have also printed at the right-hand side individual drops, with a diameter on the substrate of 70 ± 3 μm. With this diameter and the size of an individual drop we find with (4) that the contact angle is very close to the advancing contact angle of the liquid on the substrate.

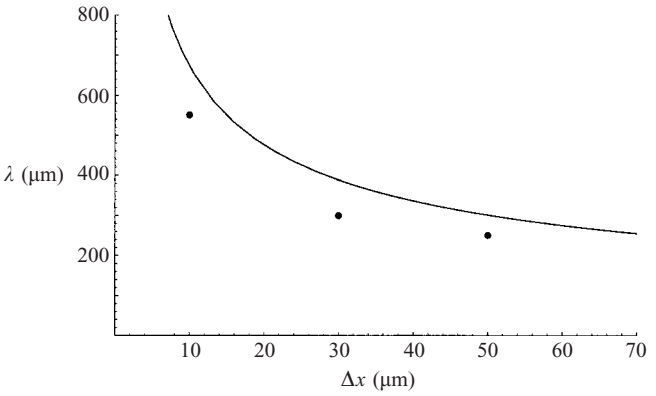

FIGURE 4. Wavelength of the instability for finite θ_r, as a function of Δx. The theoretical formula (5) of Schiaffino & Sonin (1987) is compared with the experiments.

The drops printed at an inter-drop distance smaller than the individual drop diameter do not merge to a stable line but instead the line breaks up into individual drops, i.e. the liquid dewets the substrate. Therefore every dot on the substrate contains the volume of many ink-jet printed droplets, e.g. for figure 3(*a*) about 10 droplets. The wavelength between these drops, λ, increases with decreasing Δx. This was found to occur for all printed drops, at all possible substrate velocities. Note that the droplets are not spherical, probably due to the difference in θ_a and θ_r.

This instability was observed by Schiaffino & Sonin (1997), for water printed on a Plexiglas substrate. The important aspect of this instability is that the liquid must have a finite receding contact angle, preferably close to the advancing contact angle. This is easier to achieve with a pure liquid than with a suspension. With e.g. a CF_4 plasma, however, this can be obtained for a suspension as well.

The instability can be described theoretically with a boundary condition of a constant contact angle, as was reported by Davis (1980) and Schiaffino & Sonin (1997). The line is unstable for all contact angles θ. The wavelength of the instability is a function of θ. To compare our experimental results with the one-dimensional stability theory of Schiaffino & Sonin (1997), we use a constant contact angle of $\approx \pi/2$, see table 1. The theoretical results then give $h/\lambda \approx 0.15$, with h the height of the stable liquid line. With (3) and (2) and the standard relation for a truncated circle we can easily find that the theoretical relation for the wavelength of the drops becomes

$$\lambda \approx \frac{1}{0.15}\sqrt{\frac{2V_d}{\pi \Delta x}}. \tag{5}$$

The wavelength scales with the inverse square root of the inter-drop distance, which was found to hold reasonably in the experiments. Further, figure 4 shows that the absolute wavelength is also in reasonably good agreement with the theory.

4. Experiments with a zero receding contact angle boundary condition

These experiments were performed with the standard substrates and the UV–ozone cleaned substrates. For both substrates $\theta_r = 0$; the only difference is in θ_a, which is much lower for the UV–ozone treated substrates (see table 1).

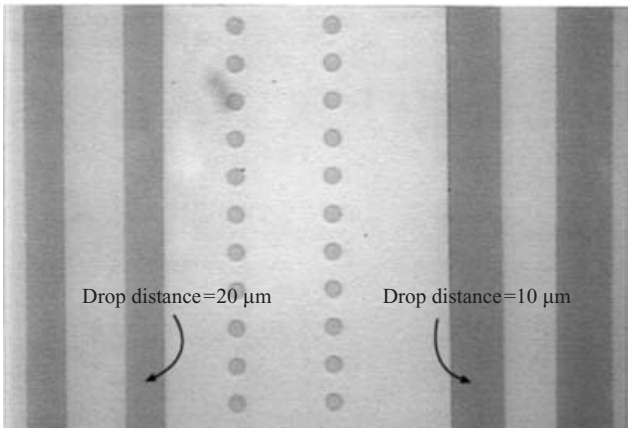

FIGURE 5. Ink-jet printed 'stable' lines on a type I substrate, with different Δx and substrate velocity of $5\,\mathrm{mm\,s^{-1}}$. In the middle of the figure single drops with a diameter of 165 μm on the substrate are shown.

4.1. *Experiments with UV–ozone treated substrates*

On the UV–ozone treated substrate almost all printed lines were stable, i.e. the drops merged together to a perfectly straight line, figure 5. In the middle of this figure the individually printed drops can be observed, with a diameter of 165 ± 3 μm on the substrate. At the side of the figure the drops were printed at an inter-drop distance, Δx of 10 and 20 μm, respectively.

Let us first discuss the printing of a single drop on a substrate. After hitting the substrate it takes some time before the drop reaches equilibrium. This is mainly due to shape oscillations of the drop as was also observed by Attinger, Zhao & Poulikakos (2000) for an ink-jet printed hot metal drop on a substrate. A typical time scale, T_0, is the $n = 2$ mode surface oscillation of a drop, as given by Lamb (1932):

$$T_0 = \frac{1}{2\pi}\sqrt{\frac{8\rho A^3}{\sigma}}, \tag{6}$$

which gives for our problem $T_0 \approx 1 \times 10^{-5}$ s, too fast to be observed with our CCD camera.

When a 'stable' liquid line is printed there are more time scales involved. First, there is that of a single drop landing in the line, which is similar to (6). After this very short time when the oscillations are damped out the line will spread from an initial width to a final width. For simplicity we assume that the initial width at the start of this process is equal to the width of a single drop. Because the area of the cross-section is known from (3) we can calculate with (2) the contact angle θ_1 of the liquid with the substrate at the start of spreading. At sufficiently small Δx the contact angle θ_1 will be larger than θ_a. Then the capillary forces will cause the line to spread until the equilibrium contact angle θ_a is obtained, figure 6. With (2) and θ_a the width of all stable lines can be calculated and were found to be in perfect agreement with the experimentally determined line width. The width of the 10 μm inter-drop distance line was found to be exactly $\sqrt{2}$ larger than the lines with inter-drop distance of 20 μm, as follows also from (2) and (3).

The time scale for capillary spreading of a line is much larger than T_0. It is a complicated problem, due to the moving liquid front. Here we will use the molecular

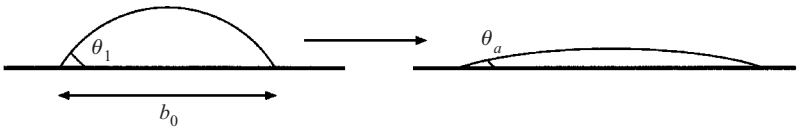

FIGURE 6. Cross-section of the spreading of a 'stable' line due to capillary forces. A line with an initial contact angle θ_1 and width b_0 (equal to the width of a single ink-jet printed drop) spreads to the equilibrium width given by θ_a.

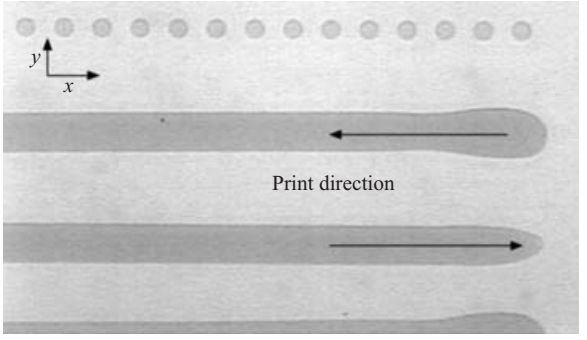

FIGURE 7. End effects on a type I substrate of a 'stable' printed ink-jet line. Substrate velocity $5\,\mathrm{mm\,s^{-1}}$, $\Delta x = 50\,\mu\mathrm{m}$. The diameter of the single drops is $165\,\mu\mathrm{m}$.

displacement approach by Blake (1993). The relation between the velocity of a moving liquid front, v, and the dynamic contact angle, $\theta(t)$, is given by his equation (22), which is

$$v = \frac{K_1}{\mu} \sinh \frac{\sigma(\cos\theta_a - \cos\theta(t))}{K_2}, \tag{7}$$

where K_1 and K_2 contain several constants which are explained in the paper by Blake. In our experiments it is appropriate to linearize this equation to

$$v = \frac{K_1\sigma}{K_2\mu}(\cos\theta_a - \cos\theta(t)), \tag{8}$$

which is equation (23) in Blake's paper. Figure 17 in Blake is a masterplot of μv versus $\sigma(\cos\theta_a - \cos\theta(t))$. From this plot we find for $\sigma(\cos\theta_a - \cos\theta(t)) = 0.015$ a typical moving contact line velocity of 5×10^{-4} m s^{-1}. This gives a time for spreading of the line due to capillarity of $O(0.1)$ s, which is in reasonable agreement with the spreading time observed on our video system and is much larger than the equilibrium time of a single drop.

There is also a hydrodynamic theory for the velocity of the moving contact line based on the viscous dissipation near the three-phase line, as is discussed by e.g. de Gennes (1985). This theory, however, is only valid in the limit of small contact angles.

In figure 7 the starting and stopping of printed stable lines is shown. In all experiments the lines are printed in two directions, i.e. at the end of a printed line the ink-jet head stops printing, the stage is moved in the y-direction and the head starts printing again, while the stage is moving in the opposite x-direction. The lines are clearly somewhat more widened at the start, probably because in this phase the

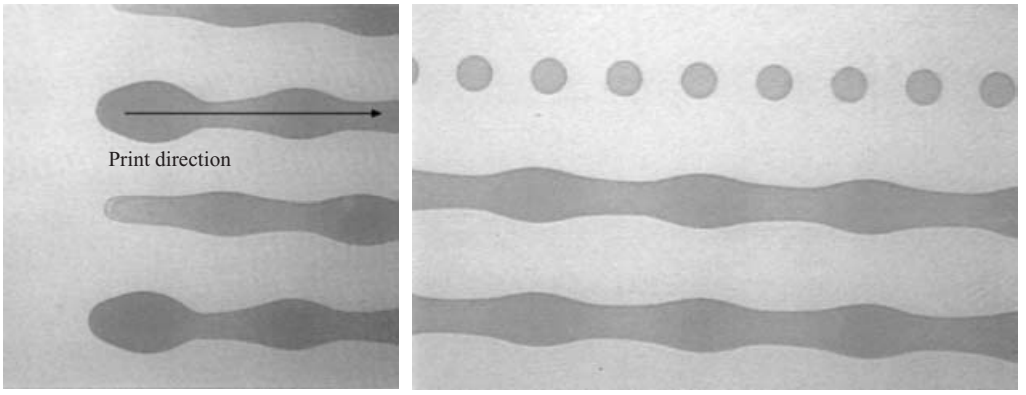

FIGURE 8. Instability of a printed liquid line on a type I substrate. Velocity of the substrate $2\,\mathrm{mm\,s^{-1}}$ and inter-drop distance $\Delta x = 50\,\mu\mathrm{m}$. The individually printed drops have a diameter of 165 μm. The left-hand figure shows the end effects of the printed line.

pattern changes from one with a truncated spherical symmetry (drop) to a truncated cylinder symmetry (line).

On a type I substrate, i.e. a UV–ozone treated plate, a printed liquid line is not always stable, figure 8. Below a critical substrate velocity, U_c, the printed line was found to be unstable, similarly to figure 1(*b*), by forming bulges connected, by a ridge of liquid. Note that the only difference between figure 7 and figure 8 is the substrate velocity U. In figure 8 the width of the ridge connecting the bulges is of similar size to the width of an individually printed drop. The instability was observed for different Δx. For the UV–ozone treated substrates $U_c \approx 3\,\mathrm{mm\,s^{-1}}$ for $\Delta x = 50\,\mu\mathrm{m}$.

We are interested in the contact angle θ_1 of the line before it starts to spread due to capillarity, when it is assumed to be equal to the width of a single drop, figure 6. With $\Delta x = 50\,\mu\mathrm{m}$ and a width $b_0 = 165\,\mu\mathrm{m}$ we find with (2) and (3) that $\theta_1 = 0.66$. This value is larger than θ_a but much smaller than $\pi/2$.

Apparently, an ink-jet printed liquid line on a type I substrate can become unstable when the contact angle of the line with the substrate is much smaller than $\pi/2$. When the substrate velocity is above a critical velocity the line is stable and the final width of the line is in good agreement with the theoretical relation (2) with $\theta = \theta_a$.

4.2. *Experiments with 'standard' substrates*

Now we move to the experiments on type II substrates, the standard untreated resist. We have observed that printed liquid lines can become unstable. The instability is of a completely different kind than the one with finite θ_r. In figure 9 we show results for printed liquid lines, all at the same substrate velocity of $2.5\,\mathrm{mm\,s^{-1}}$, for different Δx. When Δx exceeds a critical value we found that the lines can become unstable, i.e. a liquid bulge is formed connected by a ridge of liquid, similar to figure 1(*b*). At low Δx only one single bulge at the start of the line was formed, figure 9(*a*). When Δx is reduced the wavelength between the bulges rapidly decreases. Note that this instability is similar to the one observed in figure 8, i.e. bulges connected by a ridge of liquid.

We observed that the change from stable to unstable lines occurs at $\Delta x \approx 60\,\mu\mathrm{m}$. At this inter-drop distance the width of the line is still equal to the width of a single drop. For all our experiments on type II substrates $b_0 = 108 \pm 3\,\mu\mathrm{m}$. With (2) and (3) the angle θ_1 of the line with the substrate, as shown in figure 6, can be calculated,

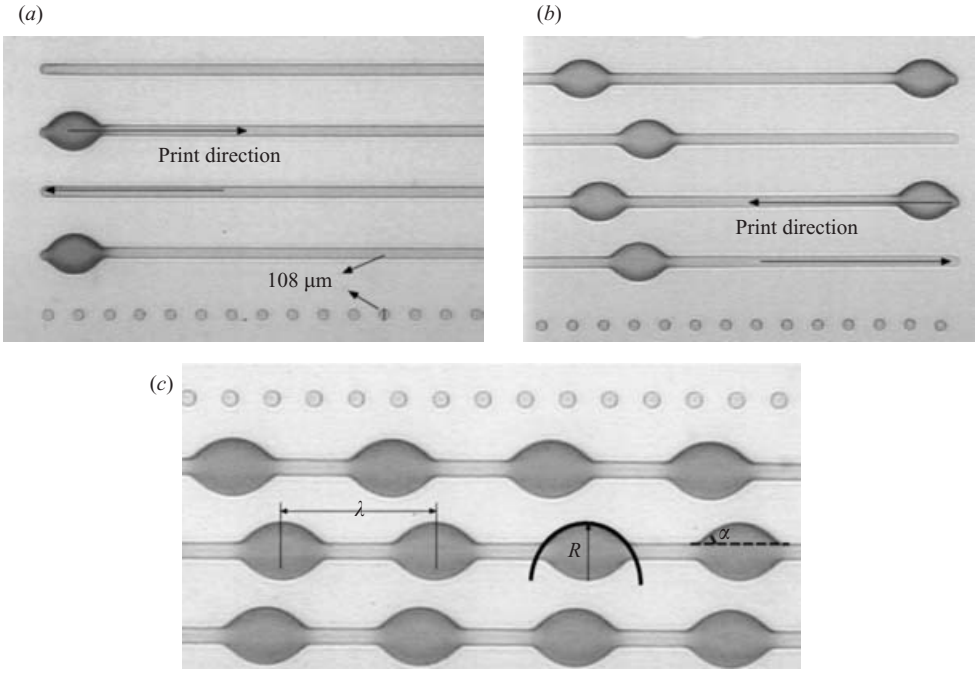

FIGURE 9. Instability of an ink-jet printed liquid line on a type II substrate with $\theta_r = 0$ and $\theta_a = 1.15$ for different Δx, all with a substrate velocity of $2.5\,\mathrm{mm\,s^{-1}}$. (*a*) $\Delta x = 50\,\mu\mathrm{m}$; (*b*) $\Delta x = 30\,\mu\mathrm{m}$; (*c*) $\Delta x = 10\,\mu\mathrm{m}$. In (*a*) and (*b*) starting and stopping of the printed lines is shown. In (*c*) two parameters to describe a bulge, R and α, together with the wavelength λ are given.

which gives $\theta_1 \approx 1.13$. The maximum error in θ_1 is 0.08 rad, which is found from a Taylor expansion of the functional relations (2) and (3). This value for θ_1 is, within the experimental uncertainty, equal to the advancing contact angle θ_a. Apparently a line can become unstable when $\theta_1 > \theta_a$.

When the printed line is unstable the width of the connecting liquid ridge between the bulges on the type II substrates was found to be exactly equal to the diameter of an individually printed drop on the substrate, b_0. The cause of the existence of the connecting liquid ridge is $\theta_r = 0$, i.e. the liquid does not dewet the substrate. Hence the width of the ridge can never become smaller than the width of a single ink-jet printed drop.

At the start of every unstable line we always observed a bulge. At this position there is a change from spherical to cylindrical symmetry. Apparently this is the 'seed' for the instability and a bulge starts to grow. The bulge consumes liquid from the printed ridge. This causes the angle of the liquid in the ridge to be lower than θ_a, i.e. the line cannot spread. The liquid can only be pumped through the ridge to the bulge by a pressure difference, which is generated here by surface tension. At the position where the printed droplets merge with the line there is extra curvature which generates an increase in pressure. This extra pressure pumps liquid to the bulge, figure 10. Because the liquid is pumped from the front of the line to the rear there is always a connecting ridge at the end of the printed liquid line.

After a particular length of the line is exceeded a new liquid bulge will grow. With increasing length of the ridge the flow rate through the ridge is decreasing. At some

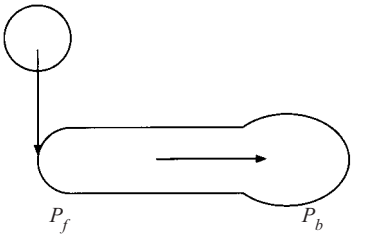

FIGURE 10. Schematic drawing of the start of the growth of a liquid bulge at the rear of a printed line. The pressure at the front of the line, P_f, is larger than in the bulge P_b, because of the extra curvature.

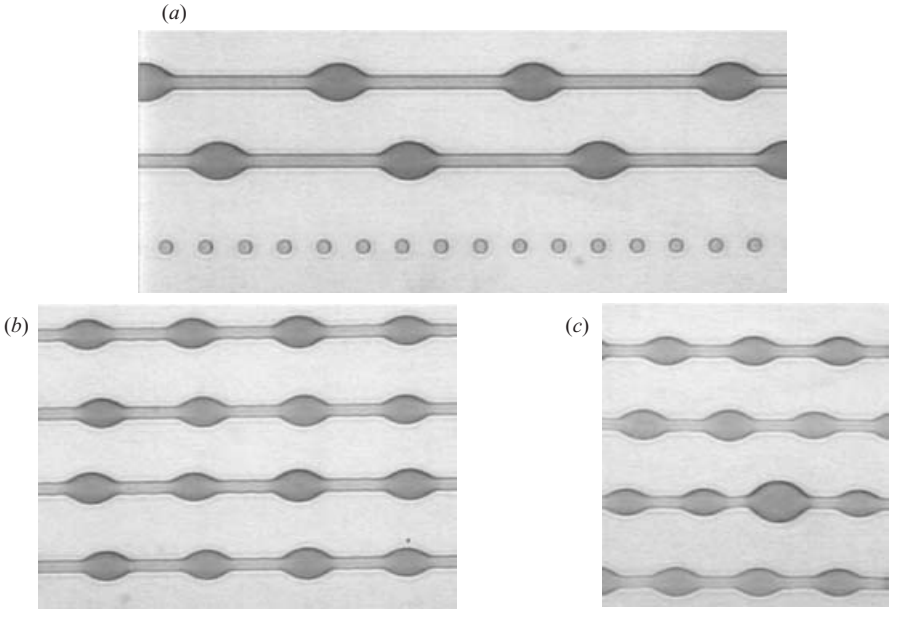

FIGURE 11. The instability of a printed liquid line for different substrate velocities, all with an inter-drop distance of 30 μm: (*a*) substrate velocity 5 mm s^{-1}; (*b*) 10 mm s^{-1}; (*c*) 20 mm s^{-1}. Note that at higher substrate velocities the size of the bulges is not completely regular. The width of the connecting ridge is 108 μm in all pictures.

point in time the contact angle of the liquid in the ridge becomes larger than the advancing contact angle. We will show that then it is favourable for a new liquid bulge to grow. It was noticed that a new bulge starts to grow at a finite distance from the front of the line where the drops are landing. This distance is very small, however, of order 300 μm, i.e. only a few times the width of the ridge. It is referred to as l_m, the minimum length of the ridge. Although the accuracy of these measurements is not very good we found that l_m decreases slightly with decreasing Δx and seems to be nearly independent of the substrate velocity.

When the substrate velocity, U, is increased at constant Δx the distance between the bulges decreases (figure 11). Due to volume conservation the bulge now becomes smaller. This was observed to hold for all cases studied with $\Delta x < 60$ μm.

All experimental pictures show a top view of the bulges. In the plane of the substrate the contour of a bulge can be described as a truncated circle with radius

R which intersects the ridge at an angle α, as is shown in figure 9. The final value of R and α is not constant but depends on Δx (figure 9) and U (figure 11). Typical values are $R \approx 300\,\mu m$ and $\alpha \approx 0.8$ rad. In all the experiments we found that the radius R is equal to the maximum width of the bulge.

The instability on the type I and II substrates, i.e. with $\theta_r = 0$, is different from the instabilities in which either the contact angle or the width is constant. The experiments on the type III substrate can be reasonably well described with a constant contact angle. With this boundary condition the wavelength between the drops increases with decreasing Δx, as is shown in figure 4. On the substrates with $\theta_r = 0$, however, the distance between the bulges decreases with decreasing Δx. Further, the distance was also found to depend on the substrate velocity. With a constant-width boundary condition a liquid line becomes unstable when $\theta > \pi/2$, as observed by Schiaffino & Sonin (1997). Our experiments on the type I and II substrates also do not match with this boundary condition.

The results show some resemblance with recent experiments by Gau *et al.* (1999) and a discussion of these experiments by Lipowsky (2001) on the stability of liquid lines on a non-homogeneous substrate. These substrates were patterned with micro-contact printing to form hydrophilic stripes on a hydrophobic substrate, where $\theta_a = 1.88$ on the hydrophobic region. By condensation a water ridge was formed on the hydrophilic stripes. Above a contact angle of $\pi/2$ the liquid stripe was unstable and one single bulge was formed that also wetted the hydrophobic area of the plate. The shape of the bulge in these experiments is similar to the bulges in our experiments. With a numerical calculation based on minimizing the free-surface energy Gau *et al.* (1999) found a good agreement between the experimentally observed and calculated shape of the bulge. The main difference with our experiments is that in these experiments a line is formed by homogenuous condensation, while in our experiments there is a moving liquid front.

We will now summarize the main points of the experiments on the type I and II substrates, i.e. with $\theta_r = 0$. First it was observed that a line may become unstable when $\theta_1 > \theta_a$. The instability is completely different from the instability with known boundary conditions. The condition $\theta_1 > \theta_a$, however, is not a sufficient condition for instability, as was observed on the type I substrates. Apparently, for this substrate type the velocity of the substrate must be lower than a critical value. In the next section a simple model is developed to describe the observed phenomena.

5. Dynamical model for instability of a line with zero receding contact angle

A classical approach for stability problems is to perform a linear stability analyis of the unperturbed problem, e.g. Davis (1980) and Schiaffino & Sonin (1997). Due to the non-symmetric boundary condition of our problem, where the contact line can only advance and not recede, this approach is not suitable. Therefore another, simple, approach has been used. First we derive a condition for stability of a line with zero receding contact angle. With a simple model the dynamics of the bulge formation is studied. Finally we discuss the stability of a line on a type I substrate.

In our model we assume for simplicity that the viscosity remains constant. This assumption is reasonable when the typical time of the experiment is much smaller than the typical time for evaporation. Further, the influence of surface tension gradients is neglected, i.e. a constant surface tension is assumed. We can use a simple argument to support this assumption. During printing of a line the polymer concentration at the front of the line, where the drops land, will be slightly lower than further

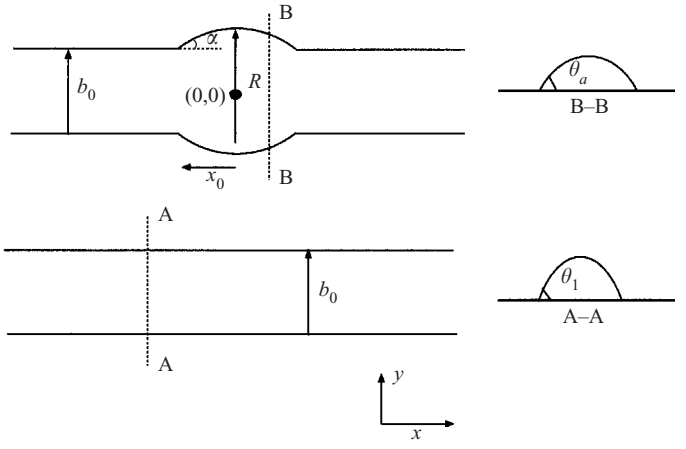

FIGURE 12. Top view of a stable line with a constant cross-section with contact angle θ_1, and a line with a small disturbance (bulge). The contact angle of the liquid in the disturbance is equal to θ_a.

down the line, due to evaporation. As the surface tension decreases with increasing concentration, this will give a somewhat larger surface tension at the front of the line, resulting in a flow directed to the front of the line. This is in the opposite direction to that observed in the experiment. Therefore it seems reasonable to neglect the influence of a surface tension gradient.

Before starting the modelling we should briefly describe the different contact angles that are used. These are θ_a and θ_r, the advancing and receding contact angle which follow from the quasi-static measurements as described in table 1. Further, there is θ_1, which is the contact angle of a stable line with width b_0, as given in figure 12. When a line is unstable θ_2 is the contact angle in the ridge connecting the bulges.

5.1. *Static condition of stability for a liquid line with zero receding contact angle*

It is our intention to derive a condition for stability for a line of liquid with zero receding contact angle. Therefore we start with a stable line with a width equal to the width of a single printed drop, b_0, i.e. a line where there is no disturbance of the impacting drop and the line has not yet spread due to capillarity. This line has constant cross-section with angle θ_1, which can be experimentally varied by changing Δx. The line will be unstable when the pressure in a small disturbance (bulge) is smaller than the pressure in the line. The condition $\theta_r = 0$ indicates that a disturbance can only increase the line width as is shown in figure 12. Further, we assume for simplicity that the liquid in a disturbance spreads with the advancing contact angle, as given in table 1, i.e. we assume a quasi-static situation. This assumption will be discussed later.

Based on our experiments we model the shape of the bulge in a very simple, geometric way. In the plane of the substrate the contour of the bulge can be described as a truncated circle with radius R which intersects the ridge at angle α, figure 12. The contour $b(x)$ of a bulge on the substrate is then given by

$$b(x) = b_0 + 2(\sqrt{R^2 - x^2} - R\cos\alpha), \qquad -x_0 \leqslant x \leqslant x_0, \tag{9}$$

$$x_0 = R\sin\alpha, \tag{10}$$

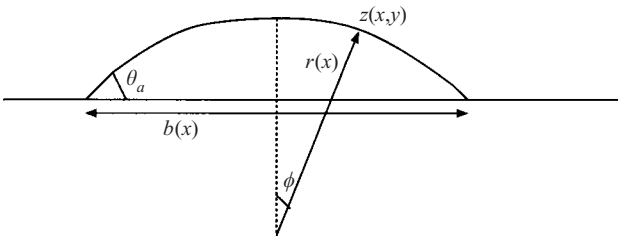

FIGURE 13. Cross-section of the bulge at position $b(x)$ with radius of curvature $r(x)$.

where x_0 is half the width of the bulge, as drawn in figure 12. Due to the small dimensions we assume that the cross-section at each position on the bulge $b(x)$ can be described as a truncated circle, figure 13. The contact angle of a cross-section is not constant but changes from θ_a at $(0,0)$ to θ_2 at the point where the bulge meets the ridge. Here θ_2 is the contact angle of the ridge. To further simplify the mathematics we assume that the contact angle for each cross-section B–B is equal to θ_a, figure 12 and figure 13, as the differences between θ_a and θ_2 will be small. Our simple model with (9) is continuous in the plane of the substrate. There is, due to the difference between θ_2 and θ_a, a discontinuity of the height h of the line at the contact point between the liquid ridge and the bulge. Because this 'matching' zone is only very small, of order 5–10 μm, the difference between the exact solution and our model will be small, as follows also from figure 9(*c*).

The volume of the bulge, V_b, is a function of b_0, θ_a, R and α. It can be found by integrating the area of a cross-section (2), where the width of a cross-section of the bulge is given by (9); this results in

$$V_b(R,\alpha) = \frac{\theta_a - \sin\theta_a\cos\theta_a}{4\sin^2\theta_a}\left(2b_0^2R\sin\alpha + 4b_0R^2(\alpha - \sin\alpha\cos\alpha)\right.$$
$$\left. + 8R^3\left(\sin\alpha - \alpha\cos\alpha - \tfrac{1}{3}\sin^3\alpha\right)\right). \tag{11}$$

The total volume of a stable liquid line, V_t, with length L and contact angle θ_1 can be found from (2) or (3):

$$V_t = \frac{b_0^2(\theta_1 - \sin\theta_1\cos\theta_1)}{4\sin^2\theta_1}L = \frac{V_d}{\Delta x}L. \tag{12}$$

The pressure in a liquid line, P_l, with width b_0 and angle θ_1 is

$$P_l = \frac{2\sigma\sin\theta_1}{b_0}. \tag{13}$$

The pressure in the bulge is calculated for the static case, i.e. we assume that the contribution due to flow in the bulge is negligible. We first specify the surface of the bulge by the function $z(x, y)$:

$$z(x, y) = \sqrt{r^2(x) - y^2} - r(x)\cos\theta_a, \tag{14}$$

where $r(x)$ is the radius of curvature of a cross-section of the bulge (figure 13), which can be written as

$$r(x) = \frac{b(x)}{2\sin\theta_a}. \tag{15}$$

In the static situation the pressure at a point on the bulge is given by

$$P(x, y) = \sigma(1/R_1 + 1/R_2), \tag{16}$$

where R_1 and R_2 are the main radii of curvature at a point (x, y) on the surface. From analytical geometry it is known, e.g. Aris (1962), that the divergence of the normal vector at point (x, y) is equal to the sum of the radii of curvature, $\nabla \cdot \boldsymbol{n} = 1/R_1 + 1/R_2$. Hence the pressure in the bulge is different at every point on the bulge, which is physically not correct but caused by the simple geometric shape we assume. Therefore we define an average pressure in the bulge as

$$P_b = \frac{1}{A_b} \int_A P(x, y)\, \mathrm{d}A, \tag{17}$$

where A_b is the area of the bulge in contact with air. This gives

$$P_b = \frac{4\sigma}{A_b} \int_0^{x_0} \int_0^{b(x)/2} (\nabla \cdot \boldsymbol{n}) \sqrt{1 + \left(\frac{\mathrm{d}z}{\mathrm{d}x}\right)^2 + \left(\frac{\mathrm{d}z}{\mathrm{d}y}\right)^2}\, \mathrm{d}x\, \mathrm{d}y. \tag{18}$$

The calculation can be simplified by applying a coordinate transformation from $(x, y) \rightarrow (x, \phi)$, figure 13. This gives

$$P_b = \frac{4\sigma}{A_b} \int_0^{x_0} \int_0^{\theta_a} 1 + \frac{r'^2(x) \sin^2\phi \cos^2\theta_a - r(x) r''(x)(1 - \cos\theta_a \cos\phi)}{1 + r'^2(x)(1 - \cos\theta_a \cos\phi)^2}\, \mathrm{d}x\, \mathrm{d}\phi, \tag{19}$$

where $r'(x)$ is the derivative of $r(x)$ with respect to x.

The surface area of the bulge in contact with air, A_b, is given by

$$A_b(R, \alpha) = 4 \int_0^{x_0} \int_0^{b(x)/2} \sqrt{1 + \left(\frac{\mathrm{d}z}{\mathrm{d}x}\right)^2 + \left(\frac{\mathrm{d}z}{\mathrm{d}y}\right)^2}\, \mathrm{d}x\, \mathrm{d}y. \tag{20}$$

With the coordinate transformation $(x, y) \rightarrow (x, \phi)$ it can be shown that the area A_b can be expressed in these new variables as

$$A_b = 4 \int_0^{x_0} r(x) \int_0^{\theta_a} \sqrt{1 + r'^2(x)(1 + \cos\theta_a \cos\phi)^2}\, \mathrm{d}x\, \mathrm{d}\phi. \tag{21}$$

Substituting (15) and (9) in (21) this integral can be calculated numerically with the software routine *Mathematica* (Wolfram Research Inc.) and (19) was also calculated numerically with this.

In this static consideration we allow, for generality, every (R, α) combination. First the situation where $\theta_a < \pi/2$ is discussed. Let us assume $\theta_1 = \theta_a$. Then a small disturbance will consume some of the adjacent liquid in the ridge. We overestimate the pressure in the ridge by assuming that the contact angle remains θ_1. This is acceptable in the limit of a small disturbance volume, i.e. $\alpha \rightarrow 0$. We find that the pressure in the bulge is smallest at the position $(x, y) = (0, 0)$, using a simple analytical expression:

$$P_b(0, 0) = 2\sigma \left(\frac{\sin\theta_a}{b_0 + 2R(1 - \cos\alpha)} + \frac{(1 - \cos\theta_a)}{R \sin\theta_a} \right). \tag{22}$$

In the limit $\alpha \rightarrow 0$ the pressure in the bulge is always larger than the pressure in the line, P_l; hence this is a stable situation. Note that for $\theta_1 = \theta_a$ expression (22) is equal to the result obtained when the contact angle of a cross-section is not constant.

In the situation $\theta_1 < \theta_a$ we can use a similar argument to show that the line is stable. The minimum pressure in the bulge given by (22) is always larger than P_l, given by (13); hence the line is stable.

R (m)	α	ΔP (Pa)
0.000150	0.323	−88.1
0.000175	0.299	−44.8
0.000200	0.279	−12.3
0.000225	0.263	+13.0
0.000250	0.250	+33.2

TABLE 2. Calculation of the pressure difference between the bulge and the ridge for different (R, α) combinations. The calculations were performed for $\theta_1 = 1.3$, $\theta_a = 1.15$ and $b_0 = 108\,\mu$m.

When $\theta_1 > \theta_a$ the argument used in the previous two cases does not hold. In this situation a disturbance does not have to be small because of volume conservation. The contact angle in the bulge, θ_a, is smaller than the contact angle θ_1 of the line; therefore it can be shown with (11) and (12) that the volume of a bulge under the constraint $\alpha \to 0$ is smaller than the volume of a stable line with equal length. To fullfil volume conservation α must be finite for each R. For every combination of α and R we can calculate the volume of the bulge and compare it with a ridge of equal length. This gives us for each R one specific α where there is volume conservation. The pressure in the bulge can be calculated for each (R, α) combination that satisfies volume conservation. Essentially it is the radius of the contour of the bulge on the substrate R that is the dominant factor. When $\theta_1 > \theta_a$ we can always find a value of R that is sufficiently large for the pressure in the bulge to be smaller than the pressure in the ridge. Hence the situation when $\theta_1 > \theta_a$ is unstable, i.e. a small disturbance in line width can grow, which is in agreement with the experiments.

In table 2, we have calculated for a specific case, $\theta_1 = 1.3$, different combinations of (R, α) where volume conservation holds. The pressure difference $\Delta P = P_l - P_b(0, 0)$ is negative for small R, i.e. stable, and for a certain critical R it becomes positive, hence unstable. These calculations give for every $\theta_1 > \theta_a$ a critical R where the line becomes unstable. Note that although the initial disturbance is, due to volume conservation, finite the absolute value of the disturbance is still small. Further, if we use the average pressure in the bulge, a slightly larger critical value of R is obtained.

In this simple analysis we have neglected the spreading of the complete line due to capillarity. When $\theta_1 > \theta_a$ the line will also spread until θ_a is obtained, as was observed in the experiments shown in figure 5. Here we assume that the time scale for spreading is much slower than the time scale for bulge formation. This will be discussed in the next sections.

When $\theta_a > \pi/2$ the situation is changed somewhat. Then, until $\theta_1 = \pi/2$ the situation is stable, similarly to the boundary condition for a ridge with a fixed width, as discussed by Davis (1980) and Schiaffino & Sonin (1997). They show that when $\theta_1 > \pi/2$ this system becomes unstable. This is the boundary condition studied by Gau *et al.* (1999), who also found that a line becomes unstable when $\theta_1 > \pi/2$. In their system only a single bulge was observed because the line was applied instantaneously by condensation.

5.2. *Growth rate of a liquid bulge*

We consider an instable situation, $\theta_1 > \theta_a$ and $\theta_a < \pi/2$, and are interested in the growth rate of the liquid bulge. In principle, as we discussed in the previous section, the disturbance can grow when the pressure in the ridge is larger than the pressure in the bulge, i.e. when $\theta_1 > \theta_a$. In the analysis of the previous section we had not yet

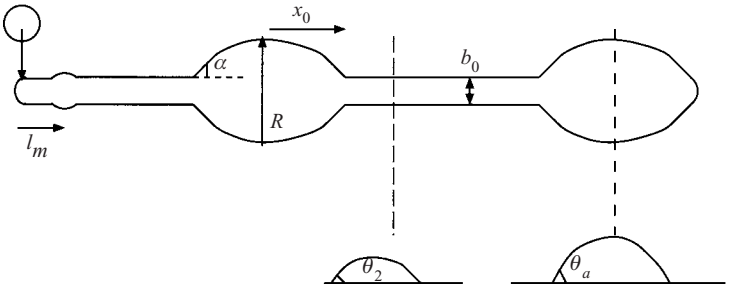

FIGURE 14. Top view of the instability, with the formation of a new bulge at the start of the line. This new bulge is assumed to start at a distance l_m from the front of the line where the drops land.

incorporated the moving liquid front, which is generated by the ink-jet printed drops on the surface.

The moving liquid front introduces an end effect in the printed line. When a line is started, the first droplets that are printed can spread a little further than the width of a single drop because there is initially a spherical symmetry, i.e. here the initial bulge starts that grows with time. In figure 14 we sketch the situation at the start of a new bulge in the line. As discussed, this bulge starts to grow at a small distance l_m from the front of the line where the printed drops are landing. At this front there is an extra curvature which generates a larger pressure P_f that can pump liquid through the ridge to the bulge. Due to the growth of the bulge the average pressure P_b in the bulge is decreasing. We assume that the pressure difference, $\Delta P = P_f - P_b$, is the driving pressure for the flow of liquid through the ridge, figure 10. With this simple assumption the growth of a bulge can be analysed; we are not restricted to small perturbations, as is the case in the linear stability analysis used by Davis (1980) and Schiaffino & Sonin (1997). In the calculations the width of the connecting liquid ridge remains constant, b_0. The contact angle in the bulge is assumed to be equal to θ_a, the advancing contact angle, and the contact angle in the connecting ridge is given by θ_2, which is assumed for simplicity to be constant in the ridge.

In our model it is important to describe the bulge with only one single dynamic variable. Here we use the radius of the contour of the bulge on the substrate, R. From our experimental results it was found that R was always equal to the maximum width of the bulge, i.e. $b(0)$. With (9) it can be shown that then there is a direct relation between α and R:

$$\alpha = \arccos\left[\frac{R + b_0}{2R}\right]. \tag{23}$$

For simplicity we assume that this relation holds during the growth of the bulge. Note that this means that we start with an infinitesimally small disturbance when $R = b_0$ because then α and x_0 are zero, as follows from (23) and (10).

It is assumed that the flow through the liquid ridge to the bulge is fully developed and viscous forces are dominant over inertia forces. These assumptions will be verified. The transported flow rate, Q, of liquid through the ridge can be written in a general form (Berger 1963) as

$$Q = \frac{s\Delta P S^2}{\mu l_r}, \tag{24}$$

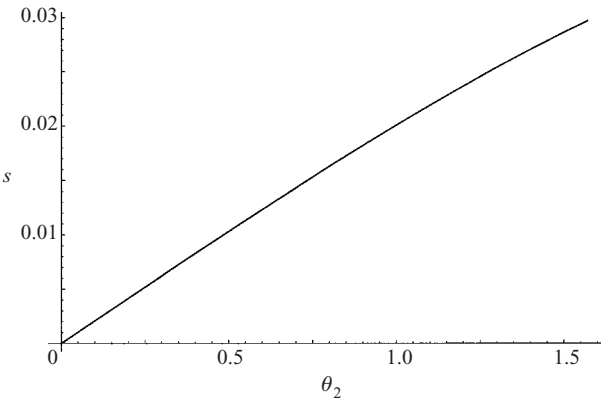

FIGURE 15. Shape factor s as a function of the contact angle θ_2.

where s is a shape factor depending on the shape of the cross-section, l_r is the length of the connecting liquid ridge, S is the area of the cross-section and μ is the liquid viscosity. This formula is valid for a cross-section where the no-slip condition holds on its entire boundary. In our case there is a zero shear stress condition on the free surface. We calculate the flow rate in this case with a simple one-dimensional approximation. Then the problem to solve is

$$\frac{\mathrm{d}^2u}{\mathrm{d}z^2} = \frac{-1}{\mu}\frac{\mathrm{d}P}{\mathrm{d}x}, \tag{25}$$

where u is the axial velocity in the ridge. The complete no-slip boundary condition is $z = 0$, $u = 0$ and $z = h$, $u = 0$. For the free surface the boundary condition is $z = 0$, $u = 0$ and $z = h$, $\mathrm{d}u/\mathrm{d}z = 0$. Calculation shows that the flow rate Q through the cross-section is a factor 4 larger with the free surface boundary condition; hence we have

$$Q = \frac{4s\Delta P S^2}{\mu l_r}. \tag{26}$$

This equation describes the flow of liquid through the ridge to the bulge.

The shape factor of the fully developed, stationary flow through a cross-section of a truncated circle, with angle θ_2 has been calculated numerically by Sparrow & Haji-Sheikh (1966). It can be shown that the shape factor s can be written as

$$s = \frac{32S}{c_f p^2 Re}, \tag{27}$$

where c_f is the friction factor, Re the Reynolds number and p the perimeter of the cross-section. For every angle θ_2 the product $c_f Re \approx 64$. Basically, the ratio of the perimeter and the surface the cross-section determines the shape value s. With use of (2) we find

$$s = \frac{\theta_2 - \sin\theta_2 \cos\theta_2}{8(\sin\theta_2 + \theta_2)^2}. \tag{28}$$

The shape factor s is plotted as a function of θ_2 in figure 15. Especially for small θ_2, the resistance to flow increases drastically.

One of the referees brought several papers to my attention where the problem of a steady, pressure-driven, rectilinear flow along a ridge whose free surface is an arc of a

circle is studied analytically. Allen & Biggin (1974) solved a thin-film approximation of the problem and it was verified that for all θ their solution is only 1% different from the present one, which is essentially also a thin-film approximation. Mikielewicz & Moszynski (1978) solved the exact problem with a conformal transformation. We have compared the flow rate of their exact solution, which was numerically calculated with *Mathematica* to our approximation and found that the differences are still reasonably small. For $\theta = 1.15$ the exact solution gives a 15% larger flow rate which is rapidly decreasing for smaller values of θ. Therefore our simple approximation seems appropriate.

The growth of the volume of the bulge with time, V_b, is caused by the flow of liquid, Q, through the ridge

$$V_b(R(t)) = \int_0^t Q(\tilde{t})\,\mathrm{d}\tilde{t}. \tag{29}$$

Differentiation with respect to t then gives an ordinary differential equation for the growth rate of the bulge:

$$\frac{\mathrm{d}R}{\mathrm{d}t} = Q(t)(\partial V_b/\partial R)^{-1}. \tag{30}$$

We now consider the different terms of this equation.

The expression for $\partial V_b/\partial R$ with the constraint (23) is

$$\left.\begin{aligned}\frac{\partial V_b}{\partial R} = \frac{\theta_a - \sin\theta_a\cos\theta_a}{4\sin^2\theta_a}\Bigg(&2b_0^2\sin\alpha + 8b_0R(\alpha - \sin\alpha\cos\alpha)\\ &+ 24R^2(\sin\alpha - \alpha\cos\alpha - 1/3\sin^3\alpha)\\ &+ (2b_0^2R\cos\alpha + 4b_0R^2(2\sin^2\alpha) + 8R^3(\alpha\sin\alpha - \sin^2\alpha\cos\alpha))\frac{\mathrm{d}\alpha}{\mathrm{d}R}\Bigg)\end{aligned}\right\} \tag{31}$$

$$\frac{\mathrm{d}\alpha}{\mathrm{d}R} = \frac{b_0}{R^2\sqrt{3 - b_0^2/R^2 - 2b_0/R}}.$$

The total volume of the line, V_t, is given by (12) where L is the total length of the line and θ_1 is the contact angle of a stable line. The volume in the liquid ridge, V_{lr}, is with the assumption of constant θ_2, calculated in a similar way:

$$V_{lr} = \frac{b_0^2(\theta_2 - \sin\theta_2\cos\theta_2)l_r}{4\sin^2\theta_2}, \tag{32}$$

where l_r is the length of the liquid ridge. The angle θ_2 in the ridge can be solved from volume conservation, $V_t = V_b + V_{lr}$. The length l_r is a function of time according to

$$l_r = l_m + Ut - x_0, \tag{33}$$

where l_m is the minimum length of the ridge, as sketched in figure 14, U the substrate velocity and x_0 half of the size of the bulge. The total length of the line L necessary to calculate V_t is given by $L = Ut + l_m$.

An expression for the average pressure in the bulge was derived in the previous section. With the constraint (23) the pressure in the bulge is a function of only R, for given b_0 and θ_a. We have calculated the average pressure in the bulge for our experimental situation with $b_0 = 108\,\mu\mathrm{m}$ and $\theta_a = 1.15$ numerically, figure 16. The pressure can be very well approximated by a simple analytical function:

$$P_b = \frac{1}{a_0 + a_1R(t)}, \tag{34}$$

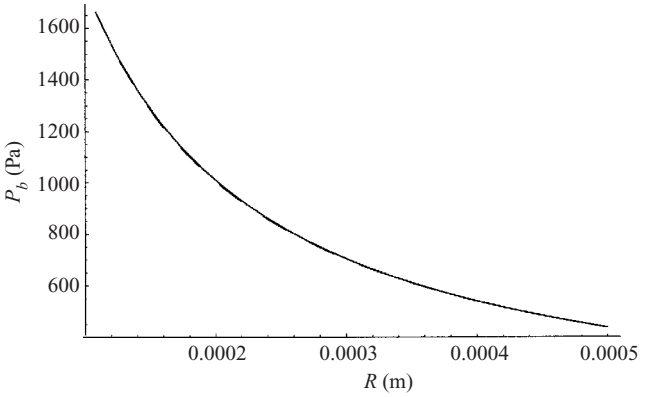

FIGURE 16. Average pressure in the bulge as a function of R for $b_0 = 108\,\mu\text{m}$ and $\theta_a = 1.15$. The full line is the numerical solution and the dashed line the simple fit (34) with $a_0 = 1.383 \times 10^{-4}$ Pa^{-1} and $a_1 = 4.287\,(\text{Pa m})^{-1}$.

where a_0 and a_1 are constants, depending only on the advancing contact angle θ_a and b_0. The fit in figure 16 was made with $a_0 = 1.383 \times 10^{-4}$ Pa^{-1} and $a_1 = 4.287\,(\text{Pa m})^{-1}$. It was found that for every reasonable b_0 and θ_a value the pressure in the bulge can be described by (34). Therefore we have used the approximation (34) in our numerical calculation for the growth rate of the bulge to calculate the pressure in the bulge.

At the front of the printed liquid line the ink-jet printed drops merge with the line. The pressure at the front, P_f, is simplified to

$$P_f = \frac{2\sigma \sin\theta_a}{b_0} + \frac{2\sigma \sin\theta_2}{b_0}, \tag{35}$$

where the first term in the right-hand side is the contribution of the individually printed drop and the second is the pressure in the ridge. We could also have taken $4\sigma \sin\theta_a / b_0$ as P_f, i.e. twice the pressure in the ridge, which was found to modify our results only slightly.

The differential equation (30) for the growth rate of R was solved numerically, combined with the volume conservation constrained to calculate θ_2. The terms in the transported flow rate Q are all a function of R, θ_2 and the constants in the experiments. These constants are b_0 and θ_a, which are for a given surface treatment and drop size fixed; and the constants that can be varied are the substrate velocity U and contact angle θ_1. With (2) and (3) the contact angle θ_1 can, for given drop separation Δx, be calculated.

The initial conditions for (30) were $R(0) = b_0$ and $\theta_2 = \theta_1$. Although not exactly correct for the first bulge, it is a reasonable approximation and can also be used for the growth rate of any other bulges formed in the line.

In figure 17 we give the growth rate of the bulge for $\Delta x = 50\,\mu\text{m}$ ($\theta_1 = 1.282$), $b_0 = 108\,\mu\text{m}$ and $\theta_a = 1.15$ for different substrate velocities. We have used for the minimum length, l_m, the experimental value of $\approx 400\,\mu\text{m}$. As can be observed, the initial growth rate of a bulge is quite fast and it is possible to pump a sufficient amount of liquid through the ridge to the bulge in a very short time.

Note that this simple model is an underestimation of the growth rate of the bulge. When the bulge is growing, the pressure in the ridge may also be larger than the pressure in the bulge; this gives an extra pressure gradient that can pump liquid to the bulge. When the length of the connecting liquid ridge is small this contribution

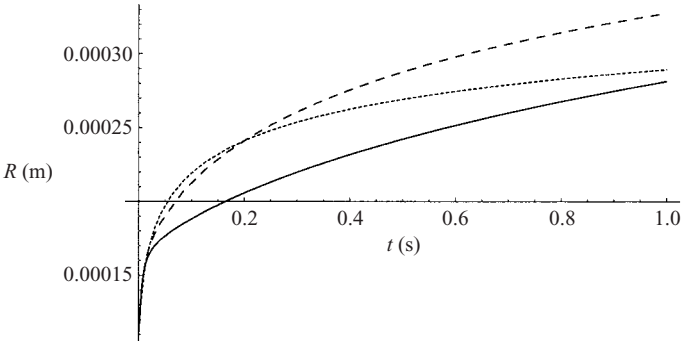

FIGURE 17. Growth of the radius R of the bulge as a function of time for $\Delta x = 50\,\mu\text{m}$ ($\theta_1 = 1.282$) for different substrate velocities. —, $U = 0.0025\ \text{m s}^{-1}$; – – –, $U = 0.01\ \text{m s}^{-1}$; $\cdots$, $U = 0.05\ \text{m s}^{-1}$.

is negligible; with increasing length of the ridge, i.e. increasing time, it will not be negligible.

We have assumed that the flow is fully developed and viscous forces are dominant over inertia forces. The average velocity, $\bar{u}$, in the ridge can be calculated with (26), where we use for simplicity $\Delta P \approx 2\sigma \sin\theta_a / b_0$. The Reynolds number of the flow in the ridge is defined as $Re = \rho \bar{u} D_e / \mu$, where D_e is given by $4S/p$, with p the perimeter. When the length of the ridge is small, e.g. equal to the minimum length l_m, we find for $l_m = 400\,\mu\text{m}$, with $S = 3 \times 10^{-9}\ \text{m}^2$ and $s \approx 0.02$, a value $Re \approx 8 \times 10^{-2}$. Hence even at the start of flow, i.e. with a small length of the ridge, it is reasonable to neglect the inertia terms.

Another assumption is that the contact angle of the liquid in the bulge is equal to θ_a, i.e. a quasi-static situation. This assumption is reasonable when the velocity of the moving contact line of the bulge is sufficiently small. In our model it is assumed that $R = b(0)$, hence a reasonable estimate of the velocity of the moving contact line in the bulge is $0.5\text{d}R/\text{d}t$. This was calculated for the parameters of figure 17, which gives a typical maximum velocity of the moving contact line of $3 \times 10^{-3}\ \text{m s}^{-1}$. With the data of figure 17 of the paper by Blake (1993) we find that this gives a small increase in θ to $\approx$1.35 rad. Note from figure 17 that this maximum velocity is only valid at the start of the bulge formation. Therefore our assumption of a quasi-static situation is quite reasonable.

5.3. *Start of a new bulge*

As we have observed in the experiments, several bulges at a very regular wavelength can be formed in a printed line. Now the distance between the bulges will be calculated with our model.

In the ridge there are always very small disturbances. When the pressure in a disturbance is larger than the pressure in the ridge this disturbance cannot grow; the disturbance is damped out immediately. Only when the pressure in a disturbance is smaller than the pressure in the ridge do we assume that a new bulge can spontaneously grow, which was shown to occur when the angle θ_2 in the ridge is larger than θ_a. Therefore we need to plot the contact angle θ_2 in the ridge for different experimental conditions. In figure 18 the angle θ_2 is plotted for similar experimental conditions as in figure 17, i.e. $b_0 = 108\,\mu\text{m}$, $\Delta x = 50\,\mu\text{m}$ ($\theta_1 = 1.282$) and $\theta_a = 1.15$ for different substrate velocities.

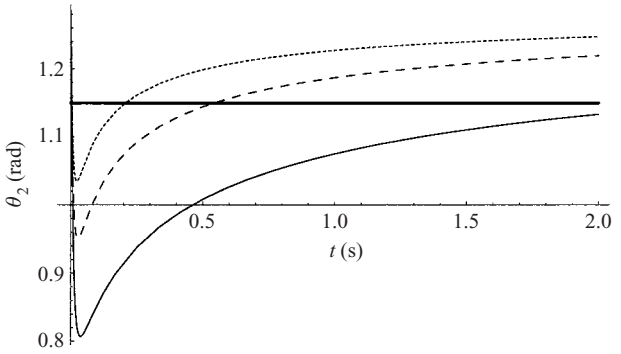

FIGURE 18. Contact angle of the liquid in the ridge, θ_2, as a function of time for $b_0 = 108\,\mu$m, $\Delta x = 50\,\mu$m ($\theta_1 = 1.282$ rad) and $\theta_a = 1.15$ for different substrate velocities., $U = 0.01$ m s^{-1}; – – –, $U = 0.02$ m s^{-1}; $\cdots$, $U = 0.03$ m s^{-1}. When the curves cross the thick horizontal line at 1.15, a new bulge can start.

Our model predicts that the contact angle in the ridge, θ_2, rapidly decreases from its initial value θ_1 to a value below θ_a. Spreading of the connecting ridge can only occur when $\theta_2 > \theta_a$, i.e. only for the first ≈ 4 ms. An approximation for the velocity of a moving liquid line as a function of the difference in contact angle is given by (8). For $\theta_1 = 1.282$ rad the constant K_1/K_2 is found from figure 17 in Blake (1993) to be $K_1/K_2 \approx 7 \times 10^{-4}$ m s^{-1}. The spreading of the ridge was calculated by numerical integration of (8) over the time $\theta_2 > \theta_a$ and found to be very small, i.e. less than 1 μm. Hence the spreading of the ridge is negligible. This means that the liquid is pumped too fast to the bulge to allow any time for spreading. The liquid also cannot dewet and therefore the width of the ridge remains constant, equal to the width of a single drop.

With increasing time, i.e. a growing length of the ridge, θ_2 is increasing again because the pressure difference for pumping the liquid to the bulge is decreasing. When θ_2 becomes larger than θ_a a new bulge can start. For a small substrate velocity this takes a long time, more than 2 s. At this time scale evaporation of the solvent will not be negligible and the constant viscosity assumption is probably not valid. This will result in only one single bulge at the start of the line, similar to figure 9(*a*). For increasing substrate velocities, U, a new bulge can be formed at a finite distance from the first bulge, as was also observed in the experiments. From figure 18 we expect to find for $U = 30$ mm s^{-1} a new bulge at $\approx$6–7 mm, in our experiments this distance was 4 mm, hence in reasonable agreement.

Note that for times when θ_2 is again larger than θ_a the solution is no longer physical because a new bulge will start to grow. From figure 17 the final radius of the contour of the bulge R can be found. For $U = 0.01$ m s^{-1} we find a growth time of ≈ 0.5 s. This gives a final radius $R \approx 300\,\mu$m, in good agreement with the experiments.

When the inter-drop distance Δx is reduced the distance between bulges decreases, figure 19. Here the drop separation was 30 μm ($\theta_1 = 1.688$ rad). Now we used $l_m = 250\,\mu$m, as found from the experiments; the other constants have similar values as in the previous figure. It can be seen that the wavelength λ between the bulges is rapidly decreasing, as was also found in the experiments. At e.g. 20 mm s^{-1} a new bulge will form at $\approx$1.2 mm, which is in reasonable agreement with the experimentally observed value of 0.8 mm, figure 11(*c*). Hence with decreasing drop distance it is more

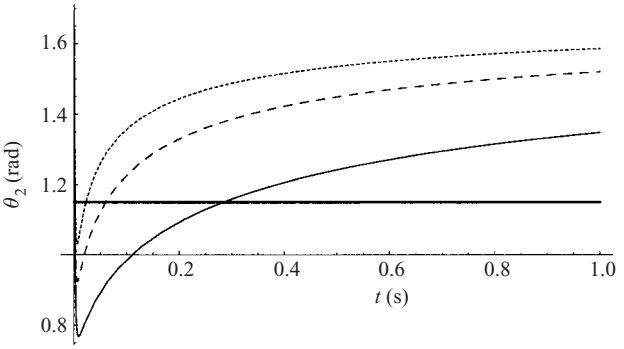

FIGURE 19. Contact angle of the liquid in the ridge as a function of time for $b_0 = 108\,\mu\text{m}$, $\Delta x = 30\,\mu\text{m}$ ($\theta_1 = 1.688$) and $\theta_a = 1.15$ for different substrate velocities. —, $U = 0.01\ \text{m s}^{-1}$; – – –, $U = 0.02\ \text{m s}^{-1}$; $\cdots$, $U = 0.03\ \text{m s}^{-1}$. When the curves cross the thick horizontal line at 1.15 a new bulge can start.

difficult to keep the contact angle in the ridge below the advancing contact angle; the wavelength between the bulges is decreasing.

When the drop separation is further reduced we can show that the wavelength for similar substrate velocities is further decreasing, in agreement with the experiment. The experiments show that even for very small Δx, it is always possible to pump enough liquid to the bulge that the contact angle in the connecting ridge is smaller than the advancing contact angle, resulting in a small connecting ridge, figure 9(*c*).

5.4. *Results for type I substrates; small advancing contact angle*

Here the results for type I, the UV–ozone treated substrates, are discussed and compared with the type II substrates.

The applied flow rate, Q_a, was similar for both substrate classes, i.e. the standard and the UV–ozone treated resist. Here Q_a is given by

$$Q_a = f V_d = SU, \tag{36}$$

where f is the frequency of drop generation and V_d the drop volume. The only difference is Q, the transported flow rate, which is much smaller for the type I substrates because θ_a is smaller. This results in a larger printed drop on the substrate (165 versus 108 μm), i.e. a larger initial line width b_0, which gives for a fixed S a smaller shape factor s and driving pressure ΔP. When we simplify the pressure difference to $\Delta P \approx 2\sigma \sin\theta_a / b_0$, we find from (26) that for $\theta_a = 0.42\,Q$ is about an order of magnitude smaller than for $\theta_a = 1.15$ at similar printing conditions, i.e. similar Δx.

When an ink-jet printed line is made with an initial contact angle θ_1 that is larger than θ_a there are two competing processes taking place. First there is the spreading of the complete line due to capillarity until the contact angle is equal to or smaller than θ_a, while the other is the growth of a small disturbance to a bulge when $\theta_1 > \theta_a$. Simply put, the first process is flow parallel to a cross-section of the line, while the second is flow perpendicular to such a cross-section. On the type II substrates the second process was shown to be dominant, i.e. spreading of the ridge due to capillarity was negligible. This is because then $Q \gg Q_a$, i.e. all the liquid that is applied at the tip of the line can be transported to the rear. On the type I substrates the transported flow is much smaller. When Q_a is increased while Q is fixed, i.e. by increasing the substrate velocity U, while Δx remains constant, it becomes more difficult to pump

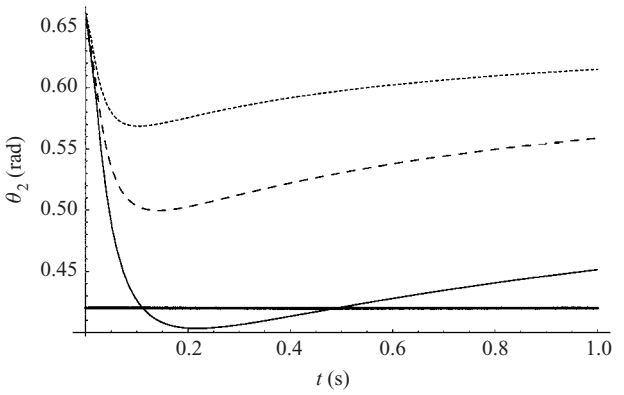

FIGURE 20. Contact angle of the liquid in the ridge, θ_2, for $\Delta x = 50\,\mu\text{m}$ ($\theta_1 = 0.66$) and $b_0 = 165\,\mu\text{m}$ on a UV–ozone treated resist with $\theta_a = 0.42$ as a function of time for different substrate velocities.—, $U = 0.002\ \text{m s}^{-1}$; – – –, $U = 0.005\ \text{m s}^{-1}$; ⋯, $U = 0.01\ \text{m s}^{-1}$. When the curves cross the thick horizontal line at 0.42 a new bulge will start.

the applied liquid to the rear to decrease the contact angle in the ridge to a value lower than θ_a. It will be shown that above a critical velocity U_c the contact angle θ_2 in the ridge is always larger than θ_a. In this situation spreading of the complete line due to capillarity will be dominant. A printed line will then have a constant cross-section, i.e. is stable, with only a small initial disturbance at the start of the line. This situation was observed for the UV–ozone treated substrates, figure 5 and figure 7. Note that due to the spreading of the line the transported flow rate is even further decreased due to the decreasing s and Δx. Only when θ_2 in the ridge becomes lower than θ_a can a pattern of bulges be formed because the ridge then cannot spread. For fixed Q this will occur when Q_a is not large enough, as is observed in figure 8.

In figure 20 the function θ_2 is plotted for the experiments on the UV–ozone treated resist with $\Delta x = 50\,\mu\text{m}$ ($\theta_1 = 0.66$), $\theta_a = 0.42$ and $b_0 = 165\,\mu\text{m}$, where b_0 is the width of an individually printed drop. We assumed an initial length before the bulge started, l_m, of 5×10^{-4} m, i.e. a few times b_0. The pressure in the bulge, P_b, is a function of θ_a, b_0 and R. With changing b_0 and θ_a we have to recalculate the fitting constants a_0 and a_1 in (34), which now become $a_0 = 8.132 \times 10^{-4}\ \text{Pa}^{-1}$ and $a_1 = 8.131\,(\text{Pa m})^{-1}$. In the calculations the width of the connecting liquid ridge was assumed to be equal to b_0. For 'large' substrate velocities, i.e. 5 and $10\,\text{mm s}^{-1}$, the contact angle in the ridge is always larger than θ_a. The applied liquid flow rate is too large for θ_2 to become smaller than θ_a. These lines will spread due to capillarity to a line with constant width, as observed in figure 5 and figure 7. Only for a low substrate velocity of $\approx 2\,\text{mm s}^{-1}$ does the angle θ_2 in the ridge become smaller than θ_a. This calculated substrate velocity is in good agreement with the experimentally observed minimum substrate velocity where bulges appear, figure 8.

From figure 20 we find a distance between the bulges for $U = 2\,\text{mm s}^{-1}$ of $\approx 1\,\text{mm}$, which is in good agreement with the experimentally observed distance of 0.8 mm, figure 8. Note that the time for θ_2 to become smaller than θ_a is much larger than in figures 16 and 17. Hence the ridge has some time to spread, as is also observed in the experiments of figure 8.

When the advancing contact angle is further decreased, e.g. by using longer UV–ozone times, or using an O_2 plasma, it becomes even more difficult for a line to become unstable, i.e. an even lower substrate velocity is necessary.

6. Conclusions

The stability of an ink-jet printed liquid line with zero receding contact angle on a flat uniform substrate was studied both experimentally and theoretically. The experiments and the simple model showed that an ink-jet printed line can become unstable when the contact angle of the liquid with the substrate is larger than the advancing contact angle θ_a. Then a small disturbance can grow into a bulge which is connected by a ridge of liquid. The pressure difference generated by the moving liquid front at the tip of the line can be sufficiently strong to pump liquid to the bulge, causing the contact angle in the ridge to be smaller than the advancing contact angle. Only when the contact angle in the ridge increases above θ_a will a new bulge start to grow. This was found to depend on both the substrate velocity and applied liquid volume, where the wavelength between the bulges decreases with increasing substrate velocity and applied liquid volume.

The condition for instability, i.e. the contact angle of the liquid with the substrate is larger than the advancing contact angle, is not a sufficient condition. When the transported flow rate through the ridge is too small with respect to the applied flow rate the line can be stable, i.e. the cross-section of a printed line is constant. Then the contact angle in the ridge is always larger than the advancing contact angle and the line spreads due to capillarity to its equilibrium width. The main dominant factor is the advancing contact angle of the liquid with the substrate. For small advancing contact angles the transported flow rate is strongly decreasing, which makes it more difficult for an ink-jet printed line to become unstable. Only at very low substrate velocities is there enough time for the line to become unstable.

I would like to thank my colleagues M. M. J. Decré, J. F. Dijksman and H. P. Urbach for helpful discussions.

REFERENCES

Allen, R. F. & Biggin, C. M. 1974 Longitudinal flow of a lenticular liquid filament down an inclined plane. *Phys. Fluids* **17**, 287–291.

Aris, R. 1962 *Vectors, Tensors and the Basic Equations of Fluid Mechanics*. Prentice-Hall.

Attinger, D., Zhao, Z. & Poulikakos, D. 2000 An experimental study of molten microdroplet surface deposition and solidification: transient behaviour and wetting angle dynamics. *Trans. ASME: J. Heat Transfer* **122**, 544–556.

Berger, R. 1963 Integration des equations du mouvement d'un fluide visquex incompressible. In *Handbuch der Physik VIII/2, Stromüngsmechanik II* (ed. C. Truesdell), pp. 1–384.

Blake, T. D. 1993 Dynamic contact angles and wetting kinetics. In *Wettability* (ed. J. C. Berg), pp. 251–309. Marcel Dekker, Inc.

Davis, S. H. 1980 Moving contact lines and rivulet instabilities. Part 1. The static rivulet. *J. Fluid Mech.* **98**, 225–242.

Deegan, R. D. 2000 Pattern formation in drying drops. *Phys. Rev.* E **61**, 475–485.

Duineveld, P. C., de Kok, M. M., Buechel, M., Sempel, A. H., Mutsaers, C. A. H., van de Weijer, P., Camps. I. G. J., Biggelaar, A. J. M., Rubingh, J. E. J. M. & Haskal, E. I. 2001 Ink-jet printing of polymer light-emitting devices. *Proc. SPIE* **4464**, 59–67.

Dussan, V. E. B., 1979 On the spreading of liquids on solid surfaces: static and dyanamic contact lines. *Annu. Rev. Fluid Mech.* **11**, 371–400.

Gau, H., Herminghaus, S., Lenz, P. & Lipowsky, R. 1999 Liquid morphologies on structured surfaces: from microchannels to microchips. *Science* **283**, 46–49.

de Gennes, P. G. 1985 Wetting: Statics and Dynamics. *Rev. Mod. Phys.* **57**, 827–863.

Lamb, H. 1932 *Hydrodynamics* Dover.

Lipowsky, R. 2001 Structured surfaces and morphological wetting transitions. *Interface Sci.* **9**, 109–115.

Mikielewicz, J. & Moszynski, J. R. 1978 An improved analysis of breakdown of thin liquid films. *Arch. Mech. Stos.* **30**, 489–500.

Rayleigh, Lord 1878 On the stability of jets. *Proc. Lond. Math. Soc.* **10**, 4–13.

Schiaffino, S. & Sonin, A. A. 1997 Formation and stability of liquid and molten beads on a solid surface. *J. Fluid Mech.* **343**, 95–110.

Sekimoto, K., Oguma, R. & Kawasaki, R. 1987 Morphological stability analysis of partial wetting. *Ann. Phys.* **176**, 359–392.

Shimoda, T., Kanbe, S., Kobayashi, H., Seki, S., Kiguchi, H., Yudasaka, I., Kimura, M., Miyashita, S., Friend, R. H., Burroughs, J. H. & Towns, C. R. 1999 Multicolor Pixel Patterning of Light-Emitting Polymers by Ink-Jet Printing. *Proc. Soc. Inf. Displ.* **1999**, 372–375.

Sirringhaus, H., Kawase, T., Friend, R. H., Shimoda, T., Inbasekaran, M., Wu, W. & Woo, E. P. 2000 High resolution inkjet printing of all-polymer transistor circuits. *Science* **290**, 2123–2126.

Sparrow, E. M. & Haji-Sheikh, A. 1966 Flow and heat transfer in ducts of arbitrary shape with arbitrary thermal boundary conditions. *Trans ASME: J. Heat Transfer* **88**, 351–358.

Xia, Y. & Whitesides, G. M. 1998 Soft lithography. *Annu. Rev. Mater. Sci.* **28**, 153–184.